Regulations on the hydration, morphology, and sulfate-attack resistivity of C$_3$A with micro/nano-silica particles

Pengkun Hou [a,*], Xinming Wang [b], Xiangming Zhou [a,*], Xin Cheng [c], Surendra P. Shah [d]

[a] Department of Civil & Environmental Engineering, Brunel University London, Uxbridge, Middlesex UB83PH, United Kingdom
[b] School of Civil Engineering, Harbin Institute of Technology, Harbin 150090, PR China
[c] Shandong Provincial Key Lab for Preparation and Measurement of Building Materials, University of Jinan, Jinan, Shandong 250022, PR China
[d] Center for Advanced Construction Materials, The University of Texas at Arlington, TX 76019, USA

A B S T R A C T

Micro- and nano-sized SiO$_2$ particles, i.e., silica fume (SF) and nanosilica (NS) have been extensively documented of improving the durability of concrete, but rare investigation on their specific effects on tri-calcium aluminate (3CaO·Al$_2$O$_3$, C$_3$A) reactions/performances in harsh environment has been reported. This work determined the effects of SF and NS on the hydration and hardening properties of C$_3$A-gypsum systems, and their performances under sulfate attack. Results showed that NS and SF can effectively improve the sulfate attack resistivity of the C$_3$A-gypsum systems due to the filling effect and the reduction of crystal size/morphology-induced expansion: a significant reduction of the aspect ratio (length/diameter) can be observed in the NS-added sample comparing the pure C$_3$A-gypsum system. Comparatively, SF can hardly change the morphology of ettringite (AFt), which could be due to that its bigger particle size cannot effectively block the ion migration. It is expected that these findings could contribute to the utilization of fine/ultra-fine SCMs in cementitious materials systems, especially those with high amount of aluminate phases.

1. Introduction

Regulation of the hydration and hardening properties of cement concrete with micro-/nano-particles has been regarded as one of the most prominent techniques of improving the performances of concrete structures during the last decades, especially for those served in harsh environments [1–5]. Silica-based particles are widely used for regulation properties of cementitious materials since the use of micro-sized silica fume (SF) for off-shore high performance concrete casting in Norway [6]. More recent investigations have been conducted to explore the effectiveness of nano-sized silica particles on the regulation of cement hydration [1,7–10]. It has generally been concluded that the reaction kinetics of cement [9,10], the chemical compositions/mineralogy [1,11], and the microstructure can be effectively regulated/improved [12–14] due to the seeding effect, the filling effect, and the pozzolanic reactivity of these particles.

As the most corrosive-prone constituent, aluminate phase in cements (including tricalcium aluminate (C$_3$A), calcium sulphoaluminate (CSA), aluminate phases in supplementary cementitious materials (SCMs), etc.) have attracted much more attention due to the thermodynamic instability of aluminate hydrates under the variations of the out environments (temperature [15], humidity [16]) and the inner conditions (pH [17], ion-type/concentration [18]). Meanwhile, due to the universality of aluminate phases in cement, the regulation of corresponding stages of their hydration/hardening process in cement has gained significant attention for exploring cement of superior performances (higher compactness [19], higher mineralogical/volume stability [20], higher corrosion resistivity [21], etc.). Some innovative cementitious materials, like limestone calcined clay cement (LC3) of stabilizing ettringite (AFt) with carbonaluminates [22], calcium sulfosilicate-modified CSA [23], etc. have been developed by taking advantages of the regulation of the hydration of the aluminate-phases.

Regarding the influences of SCMs on the hydration and hardening properties of aluminate phases, most researches were conducted on the CO$_3$-Al$_2$O$_3$ systems by using limestone [3]. Scrivener et al. [24] investigated the seeding effect of various sized SCMs on the hydration regulation of aluminate phases, and they believed that the aluminate phase hydration could be governed by the size of the additives. Hinted by the electrokinetic hindrance effect of Ca-S complex on the hydration retardation effect of gypsum on C$_3$A [25], Hou et al. revealed the influences

* Corresponding authors.
E-mail addresses: pengkun.hou@brunel.ac.uk (P. Hou), xiangming.zhou@brunel.ac.uk (X. Zhou).

Table 1

Physicochemical properties of raw materials.

Sample	CaO	SiO$_2$	Al$_2$O$_3$	SO$_3$	Fe$_2$O$_3$	MgO	LOI	Specific surface area (m^2/kg)
NS	–	99.8	–	–	–	–	0.2	3,000,000
SF	0.12	98.08	0.34	0.42	0.04	0.34	0.66	27,300
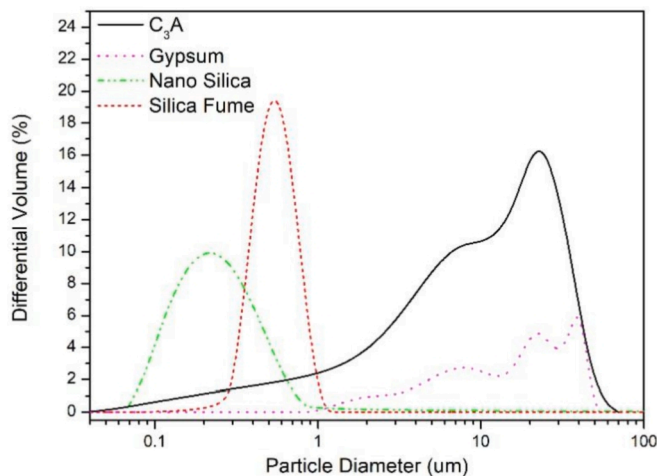
Fig. 1. Particle size distribution of raw materials.

of the surface electrical charge characteristics of micro/nanoparticles on the regulation of the hydration of C$_3$A [26,27]. It has been suggested that the negatively-charged silica particles can be attracted to the positively-charged aluminate phases, blocking the active dissolution front of C$_3$A, i.e., retarding its hydration. Maier [28], Cui [29], and Singh [30] verified the blocking effects of silica nanoparticles on aluminate phase hydration in their recent work. Moreover, this effect seems to be effective in other high aluminate-cement, calcium aluminate cement, for example, Son et al. [31] researched and proofed the hydration/hardening retardation effect of silica nanoparticles on calcium aluminate cement.

The blocking effect of silica micro/nanoparticles on aluminate phases in cement would contribute to unique influences of the behavior of cementitious materials and can be explored for better regulation of the property gain, but, to the best knowledge of the authors, this has not been researched and reported. To fill this gap, this work investigated the regulation effects of micro-/nano-sized silica particles, i.e., silica fume (SF) and nano silica (NS), on the hydration and hardening properties of the C$_3$A phase. Regulation on the sulfate attack resistivity was also determined with the hope of exploring hints for improving the durability of cement, especially those with high amount of aluminate phases.

2. Experimental

2.1. Materials

In this study, commercial tricalcium aluminate (C$_3$A, cubic, 3862 m^2/kg), obtained from DMT Materials Technology Co., Ltd, was used, in which the amount of free-CaO was less than 1 wt% (quantitative Rietveld analysis). Nanosilica (NS) and gypsum purchased from the Macklin company were of chemical grade. The chemical compositions (X-ray fluorescence), particle size distribution, and morphology of silica fume (SF) are listed in Table 1, Figs. 1 and 2, respectively. Comparison of the SEM image with the particle size distribution curve shows the

agglomeration of NS during particle size measurement. Sieved fine sand (smaller than 2 mm) was used to prepare mortar in this experiment.

2.2. Mix proportions and sample preparation

Gypsum-to-C$_3$A mass ratios of 10 wt%, 30 wt% and 86 wt% were determined according to a statistics study of the sulfur-aluminum ratio of binders of different originality for simulating different sulfation degrees [18,32,33].

2.2.1. Preparation of cement paste and mortar

Paste and mortar specimens of C$_3$A-gypsum system were prepared to investigate the effects of NS and SF on its resistance to sulfate attack. To ensure a homogeneous mixing of C$_3$A and gypsum before casting, the powder was placed in 50 mL of anhydrous ethanol, stirred at 6000 rpm for 30 min, and vacuum dried at 45 °C before been stored in a N$_2$ glove box. NS and SF were sonication-dispersed (30 min) in mixing water, and subsequently mixed with abovementioned powder to get a homogeneous paste by using an electric cantilever stirrer (300 rpm for 1 min and 600 rpm for 3 min).

Mortar specimens of cylinder shape (Φ10 mm × H20 mm) was casted for sulfate attack resistance observation. The mass ratio of sand-to-binder was 3. Powder was first drying-mixed with fine sand at 300 r/min for 1 min, and after adding the mixing water containing sonication-dispersed NS/SF, the slurry was further mixed at 600 r/min for 3 min. After casting, the mortar was covered with plastic film and moved to the curing chamber (25 °C, RH ≥ 99%) before been demolded 24 h later. The mortar samples of certain ages were moved into the 5 wt% Na$_2$SO$_4$ solution (500 mL) for sulfate attack resistivity testing.

2.2.2. Synthesis of ettringite

Ettringite, the main product of sulfate attack of the aluminate phase, was chemically synthesized using C$_3$A and gypsum for the investigation of the effects of NS and SF on the formation and evolution of ettringite. Stoichiometrically prepared C$_3$A and gypsum were prepared and mixed with deionized water (water-to-binder ratio of 1.0), and stirred thoroughly, followed by transferring the suspension to a centrifuge tube cured in N$_2$ glove box at 25 °C. After curing for 28 days, the sample was fractured and ground passing through a 74 μm sieve. The purity of the synthesized ettringite was 98% as determined by the Rietveld refinement method.

2.2.3. Sulfate attack simulation using dialysis tubing

It is considered that during the sulfate attack of hardened cement, external sulfate ions diffuse to the surface of the hydration product through pores and generate expansion. To exclusively study the intrinsic sulfate attack resistivity of the hydration products (i.e., excluding the influence of pore characteristics (porosity, tortuosity, threshold value of the ink-bottle neck, etc.) on ion diffusion), cement paste at certain curing age was ground to powder passing 200-mesh sieve (74 μm) before adding into the dialysis tube (Fig. 3). The dialysis tubing used in this experiment had a molecular weight cutoff of 10 kDa. The working principle of the dialysis tubing is comparable to the ion transport process in cement: ions transport from the location of high ion concentration to a
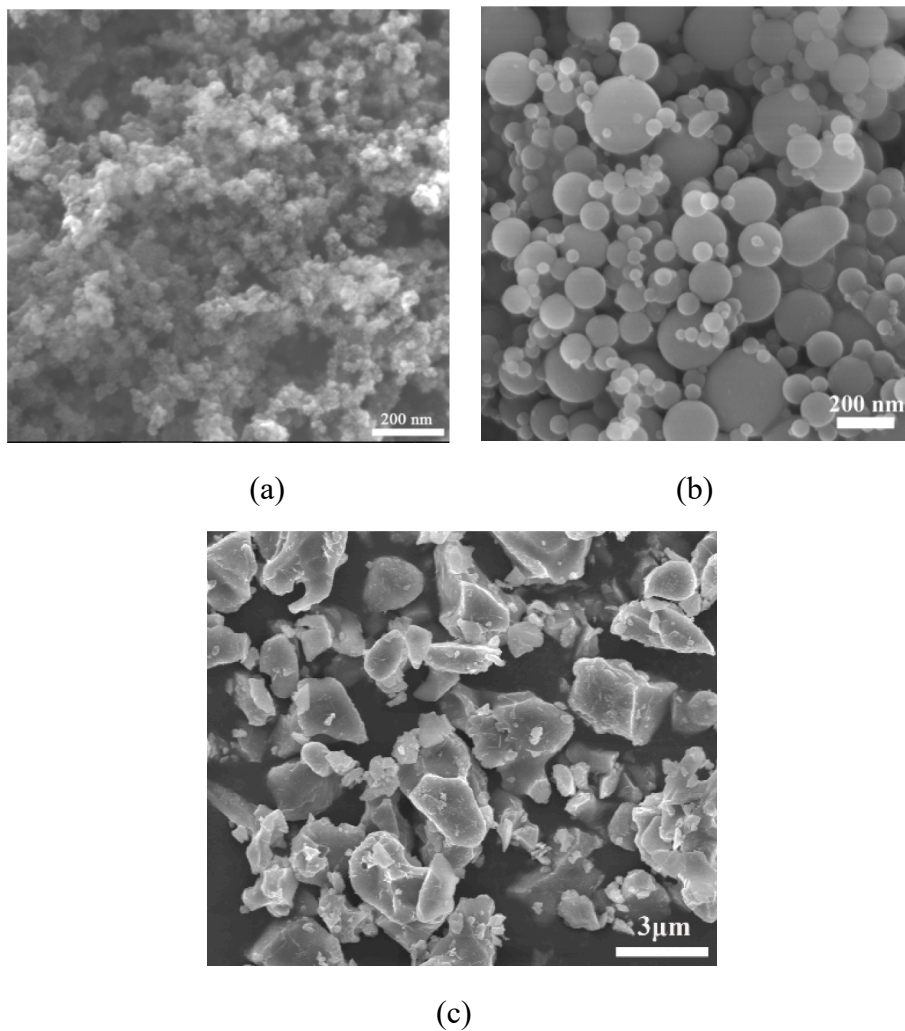
(a)

(b)

(c)

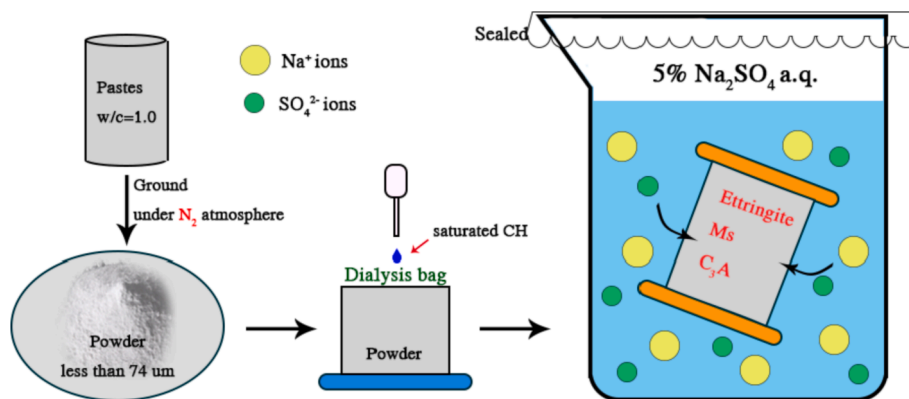**Fig. 2.** Morphology of raw materials (a) NS, (b) SF, and (c) C_3A.

Fig. 3. Schematic diagram of the sulfate attack process of C_3A paste in dialysis tubing.

low value of ion concentration. Molecules smaller than 10 kDa (SO_4^{2-}) diffuse across the dialysis membrane under its concentration gradient between the two sides of the dialysis membrane. The whole process is schematically shown in Fig. 3.

At certain age, the powder sample was taken out from the dialysis tubing and centrifuged at 8000 rpm for 2 min. Then, the supernatant was filtered off, and anhydrous ethanol was added and centrifuged twice for another 2 min. The final precipitate was moved into anhydrous ethanol

for 3 days to terminate hydration, followed by vacuum drying and sealed storage for following characterizations.

2.3. Characterization

2.3.1. Quantitative X-ray diffraction (QXRD)

D8-Advance X-ray Powder Diffraction using Cu-Kα radiation (1.541874A, 40 kV, 40 mA) with a scanning step size of 0.02° was used

Table 2
Structure information of compounds.

Compounds	ICDCS	Space group	a	b	c	Reference
C_3A, cubic	1841	Pa-3	15.263	15.263	15.263	[34]
Gypsum	409,581	C12/c1	6.284	15.200	6.5230	[35]
AFt-(ettringite)	155,395	P31c	11.229	11.229	21.478	[36]
AFm-(monosulphate)	100,138	R-3 h	5.7586	5.7586	26.7946	[37]
Monocarbonate	59,327	P1	5.7747	8.4694	9.923	[38]
Hemicarbonate	59,327	R-3c	5.7757	5.7757	48.812	[39]
Hydrated- garnet	94,630	Ia-3d	12.5731	12.5731	12.5731	[40]
ɑ-Al_2O_3	77,810	R-3cH	4.7598	4.7598	12.9924	[41]
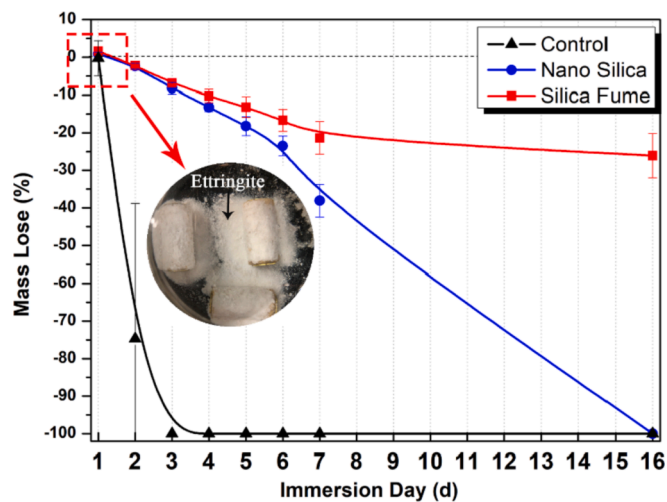
Fig. 4. The mass loss of C_3A-30 wt% gypsum control mortar under the sulfate attack.

to characterize cement paste. To quantitatively evaluate the amorphous phase, the standard internal method (ɑ-Al_2O_3) was used. Rietveld refinements were accomplished by using TOPAS 4.2 software. The refined parameters were cell parameters, zero-shift error, phase scale, and peak shape parameters using the fundamental parameters approach. Compounds considered during refinements were listed in Table 2.

2.3.2. Scanning electron microscopy (SEM)

JSM-710F field emission scanning electron microscope (Japan) equipped with an Oxford X-MaxN EDS was employed to study morphology and elemental composition of corrosion products. The length of ettringite was analyzed by Image J software. The average of 100 length data of ettringite taken from 5 different SEM images was used to determine the final result.

2.3.3. Zeta potential

The effect of NS/SF on the zeta potential of ettringite was evaluated by Malvern ZS90. Pre-dispersed NS and SF in mixed water were mixed with synthesized ettringite for 2 min, the water-to-powder ratio was 100. Supernatant after centrifuging was used for testing.

3. Results and discussion

3.1. Deterioration of C_3A-gypsum mortar containing NS/SF under sulfate attack

Unlike the sulfate attack of Portland cement, corrosion products would be rapidly generated and fall off from the surface of C_3A mortar

specimens under the 5 wt% Na_2SO_4 solution, making the mass loss suitable for assessing the degree of sulfate attack. Fig. 4 shows the results of mass loss of C_3A-30% gypsum mortar specimens during sulfate attack (three tests averaged). It can be seen that at 3 days, the control specimen was completely destroyed, while the specimens with NS/SF was only *ca.* 10%. The comparison showed that the addition of NS and SF significantly decreased the rate of mass loss of the specimens and slowed down the destruction generated by sulfate attack at early ages, which may be partially related to the denser matrix that could block the ingression of aggressive ions owing to the pore filling effect of NS and SF [5]. It may also be associated with their effects on the mineralogy evolution, which will be discussed later.

The results also showed that the rate of mass loss of NS specimens gradually increased with time, and the specimens were completely destroyed at 16 days. While for the SF specimens, the mass stabilized at 7 days and did not show a significant decrease thereafter. It can be seen that the addition of NS would accelerate the sulfate corrosion rate of C_3A-30 wt% mortar at late ages. Compared with micro-sized SF particles, the pore volume of the matrix was smaller after NS modification, which means that less space would be available for the growth of corrosion products, and the resulting larger crystalline expansion pressure was more likely leading to internal structural cracking, which in turn accelerated sulfate erosion [42].

Fig. 5 presents the images of C_3A-86 wt% gypsum mortar damaged by sulfate attack. It can be seen that at this gypsum dosage, the sulfate corrosion rate of C_3A mortar specimen was significantly increased. After 5 min, obvious cracks appeared on the surface of the control and SF specimens, which expanded rapidly with the increase of time, and the specimens were completely destroyed within 20 min. According to the XRD results, the corrosion product was ettringite; its generation amount and rate appeared to be significantly higher than that of the 30 wt% gypsum system, which will be discussed in the section on mineralogy evolution of erosion products. Results showed that the NS-modified specimens performed better compared with the control and SF specimens, and their structures were not significantly damaged until 2 h. This was consistent with the results of C_3A-30 wt% gypsum specimens, i.e., NS made the structure denser, which would hinder the migration of sulfate ions. These results showed that the content of gypsum played a vital role in the sulfate attack of C_3A specimens. Moreover, the addition of NS and SF improved the sulfate resistance of C_3A specimens could be due to their filling effect and their effects on the evolution of the corrosion product.

3.2. Mineralogy evolutions of corrosion products during sulfate attack

The quantitative mineralogy evolution of C_3A-gypsum pastes under sulfate attack calculated by QXRD is presented in Fig. 6. It can be seen that when the content of gypsum was 30 wt%, unreacted C_3A, AFm-(monosulphate, Ms) and monocarbonate (Mc) were the main hydrates after 1 day, and this result is consistent with the theoretical chemical
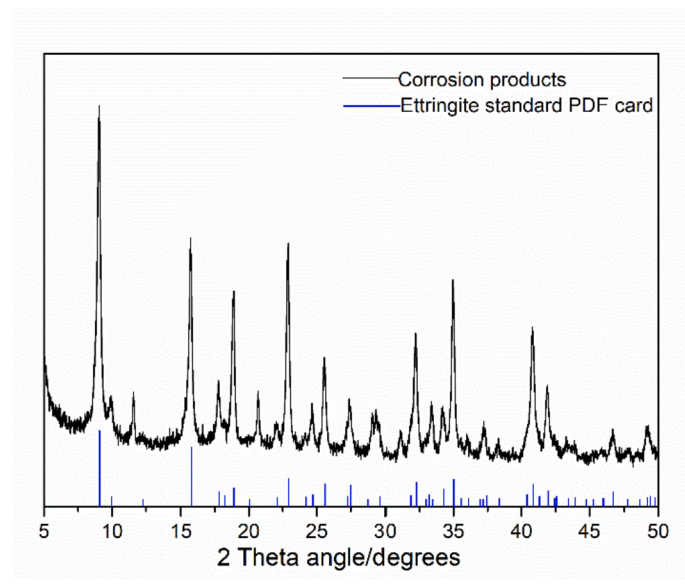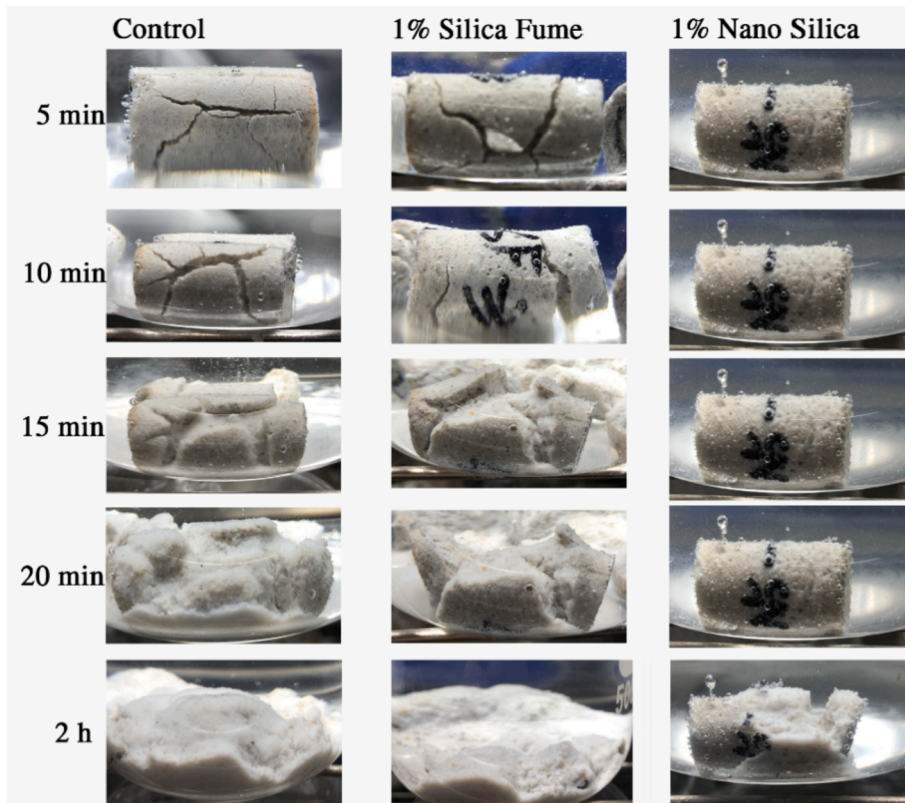
Fig. 5. Images of C_3A-86 wt% gypsum control mortar damaged by sulfate attack and XRD pattern of corrosion products.
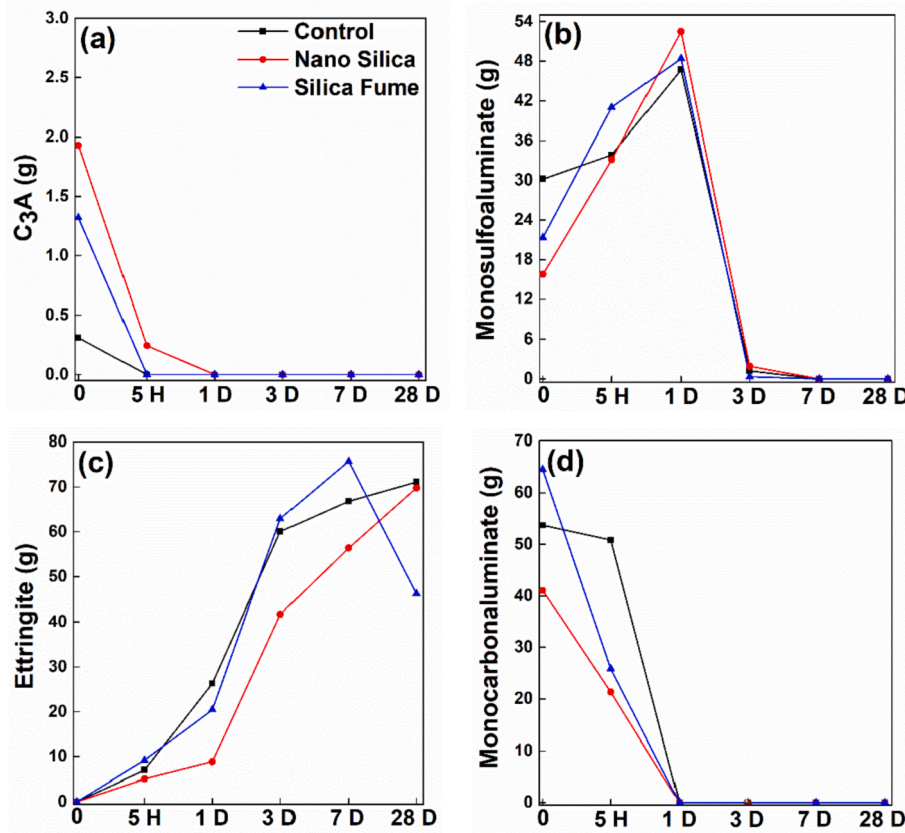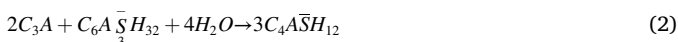
Fig. 6. Phase evolution of C_3A-30 wt% gypsum paste under sulfate attack ((a) C_3A; (b) monosulfoaluminate; (c) ettringite; (d) monocarbonaluminate, all the phase content was normalized to the absolute mass change (mass/100 g)).

reaction calculation of the C_3A-gypsum system (Eq. (1)-(2)). As for the C_3A- 30 wt% gypsum system, if we assume the gypsum dosage was 3 mol and the C_3A content should be 6.3 mol. According to the theoretical chemical equilibrium shown in Eq. (1)-(2), the whole reaction would consume all the gypsum and ettringite, whereas there was still 3.3 mol C_3A remaining and forming 3 mol Ms, which might further be carbonated to Mc as shown in Eq. (3). Unavoidable formation of monocarbonaluminate (Mc) was observed in both 30 wt% and 86 wt% gypsum-added C_3A samples. It was due to the carbonation of monosulfoaluminate (Ms) that have been introduced from the deionized water or the air atmosphere during the mixing process [43].

With the incorporation of NS and SF, an increase in the remaining C_3A content and a decrease of Ms can be clearly seen, and this hydration inhibition phenomenon is consistent with the results of previous studies, i.e., micro-/nano-SiO_2 will hinder the hydration of C_3A through the electrostatic adsorption effect and thus reduce the production of hydration products [26,27].

$$C_3A + 3C\overline{S}H_2 + 26H_2O \rightarrow C_6A\overline{S}_3H_{32} \tag{1}$$

$$2C_3A + C_6A\overline{S}_3H_{32} + 4H_2O \rightarrow 3C_4A\overline{S}H_{12} \tag{2}$$

$$C_4A\overline{S}H_{12} + CO_3^{2-} \rightarrow C_4A\overline{C}H_{12} + SO_4^{2-} \tag{3}$$

The dialysis tubing samples were then immersed in 5 wt% Na_2SO_4 solution for sulfate attack testing. It can be seen that after one day of immersion, AFt content increased significantly, which can be stemmed

from the re-hydration of the remaining C_3A or the transfer of monosulfoalumiante (Ms) [18]. In the case of high SO_4^{2-} solution, monocarbonate (Mc) turned into monosulfoaluminate (Ms) following Eq. (4). It can also be seen that AFt content decreased with the incorporation of NS. Combining with the mass loss result of the mortar sample shown in Fig. 4, it can be deduced that the improvement of the sulfate attack resistivity after NS addition could be due to both the compaction of the microstructure and the reduction of the amount of the corrosion phase. However, it can also be seen that the addition of SF did not significantly change the evolution of the phases of the C_3A sample. At 28 days, AFt content in the SF-added sample decreased sharply, which can be closely related to the consumption of sulfate ions as depicted in the C_3A-86 wt% gypsum system, and this needs more investigation.

$$C_4A\overline{C}H_{12} + SO_4^{2-} \rightarrow C_4A\overline{S}H_{12} + CO_3^{2-} \tag{4}$$

At the practically-sulfated OPC system (86 wt% gypsum), the phase evolution of C_3A paste is shown in Fig. 7. It can be seen that C_3A has depleted after 3 days of hydration with the remaining AFt. It can also be seen that the addition of NS and SF reduced the amount of AFt, Ms, i.e., retarding C_3A hydration. At 5 days sulfate attack, a fast increase of AFt happen in all the samples, to 50% of the total amount. This fast formation of expansive phases leads to the instant cracking of the sample, as shown in Fig. 5.

Comparing to the relatively slow deterioration rate of the C_3A-30 wt% gypsum system, a higher amount of AFt remained in the 86 *wt*% gypsum system (Fig. 7), leading to a more porous microstructure due to the overlapping of the needle-like AFt crystals, simplifying the transport
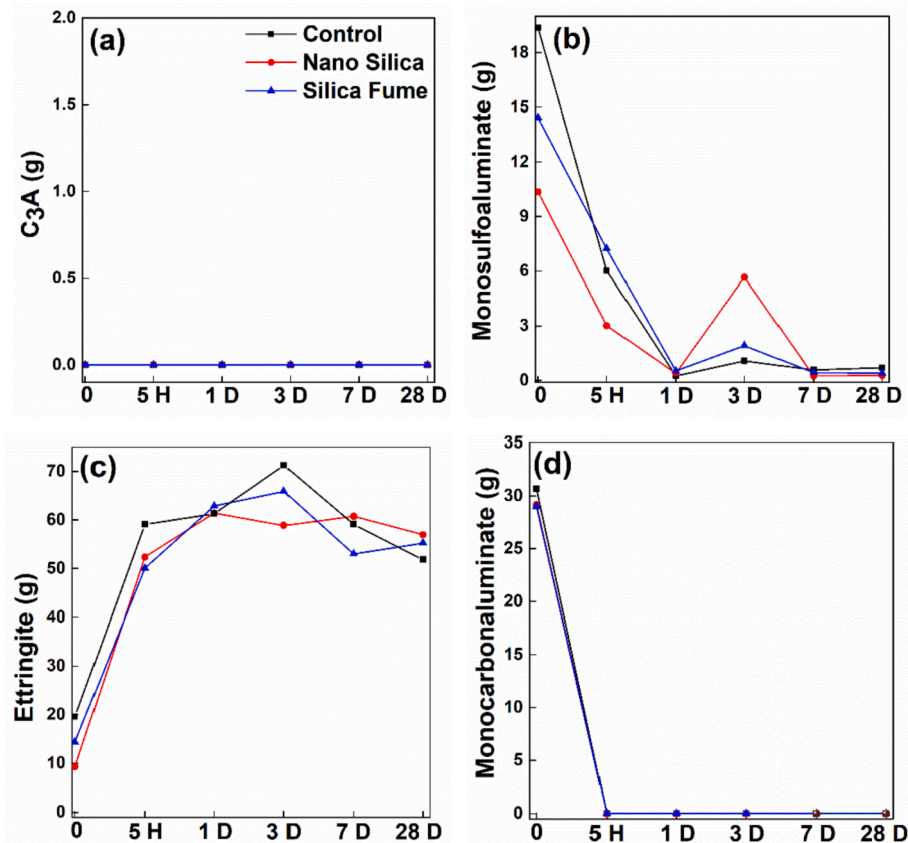
Fig. 7. Phase evolution of C_3A-86 *wt*% gypsum paste under sulfate attack ((a) C_3A; (b) monosulfoaluminate; (c) ettringite; (d) monocarbonaluminate, all the phase content was normalized to the absolute mass change (mass/100 g)).

of aggressive sulfate ions. However, the rate of this process could be lowered down at a lower gypsum content system due to the plate morphology of the hydrate of Ms favored the dense packing of the microstructure, leading to the improved sulfate attack resistivity [44].

The results also showed that the AFt content in the NS-added C_3A sample was much less than the control sample, which is comparable to the 30 *wt*% gypsum system. However, a slight reduction of AFt in the SF-added sample can be observed, and this can be due to the pore filling effect of SF. It thus can be deduced that both the early age C_3A hydration and later age sulfate attack resistivity of the C_3A sample can be influenced by NS and SF, which will be more theoretically studied in the following section.

3.3. Morphology

SEM images of C_3A samples after 28 days of sulfate attack are shown in Fig. 8. It can be seen that great variation on the AFt morphology can be achieved within samples of different sulfation degrees, NS-/SF-added samples. A statistic study of the length of AFt in the 28-day samples were conducted and compared in Fig. 9.

It can be seen in Figs. 8 and 9 that an average AFt length of 16 μm can be seen in the 30 *wt*% gypsum added sample. There is no obvious morphology change in the sample with SF addition. However, a significant variation of AFt morphology can be seen in the NS-added sample, a reduction of the aspect ratio (length/diameter) can be observed, and an average AFt length of 8 μm can be resulted. When gypsum dosage increased to 86%, the AFt length decreased to about 2 μm of short rods.

It has been reported that the morphology of AFt would potentially influence its mechanical performance: the needle-like morphology contributes to a high early-age strength, and when reduced to 2 μm, AFt will contribute no effect to mechanical strength, but to the swelling due to the adsorption of water, leading to the cracking [45].

When studying the influence of different polycarboxylate (PC) superplasticizers on the AFt morphology, Plank and the coworkers [46] proposed the selective adsorption of PC molecular on AFt leading to the change of the aspect ratio. Comparable selective adsorption of negatively charged particles (including Ca-S complex [25], nano-silica [26], and silica fume [27]) can be resulted, leading to the variant crystal length. This assumption will be more detailed investigated through the zeta potential testing, as shown in the next section.

3.4. Further discussion on adsorption

It has been well recognized that the adsorption of polymer on cement particles will potentially influence the hydration process of the latter as well as the hydration products [47]. The specific electrokinetic feature of micro/nanoparticles significantly alters its adsorption characteristics in cement, which, however, has rarely been taken into consideration during the exploration of its effectiveness. The ultra-fine particle size of nanoparticles, as well as the vast variety of the surface electrical characteristics, is of much higher importance of taking this feature into consideration of the dispersion [48], the influences on hydration/hardening properties. It has been demonstrated in the previous sections that NS' specific negatively-charged surface not only verified the
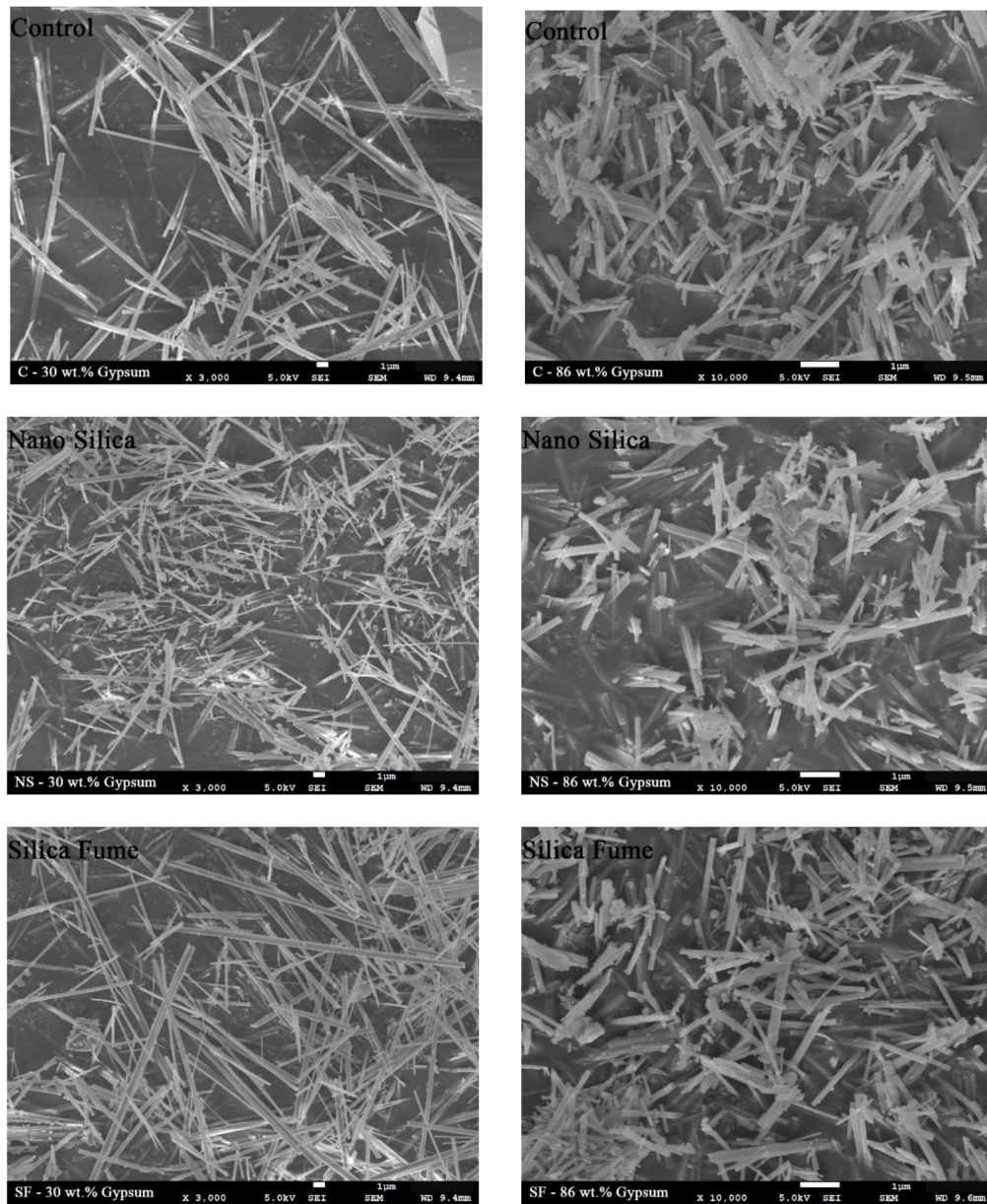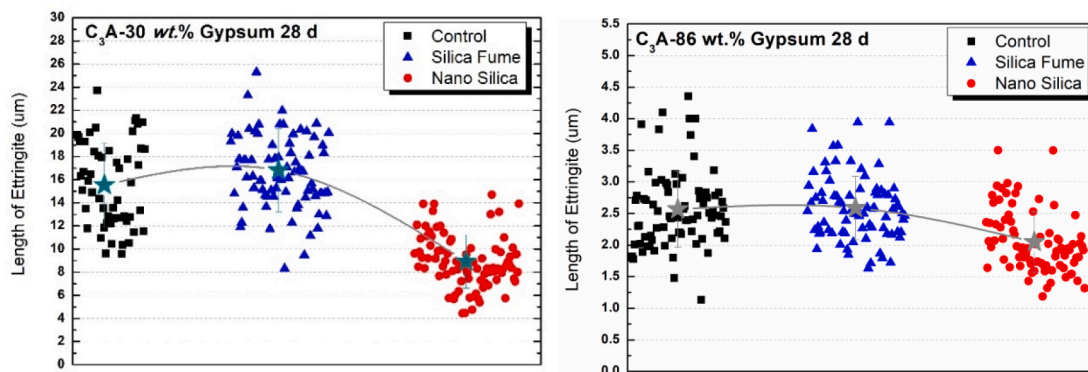
30 *wt.*% gypsum   86 *wt.*% gypsum

Fig. 8. AFt morphology in C$_3$A-gypsum systems at 28 days.

(a （C$_3$A-30*wt.*% gypsum   (b （C$_3$A-86 *wt.*% gypsum

Fig. 9. AFt length in C$_3$A paste samples of different sulfation degrees.
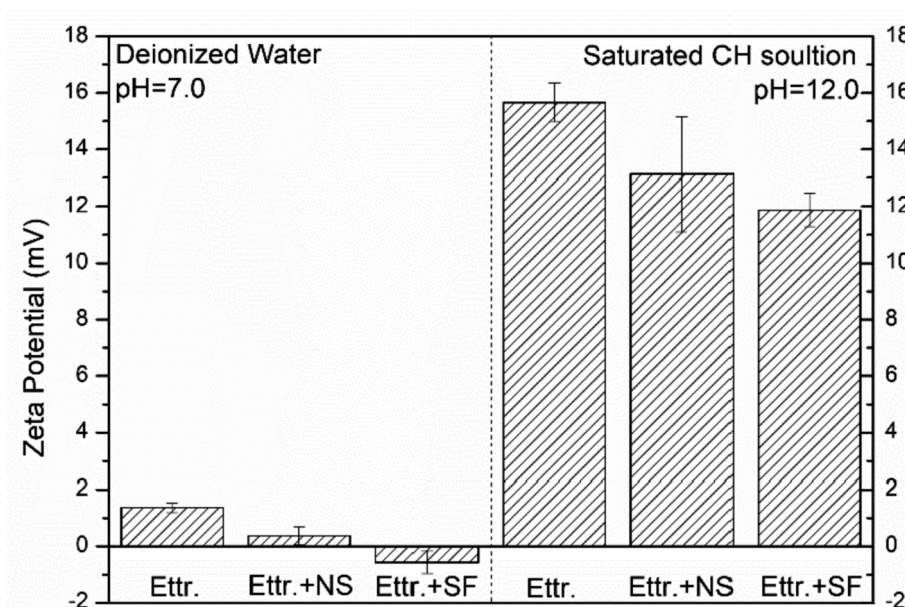

Fig. 10. Influences of NS and SF on the zeta potential of AFt (w/b = 100).

morphology of the hydration products of C$_3$A but also affected the macro-property.

The adsorption behavior of NS and SF on the C$_3$A surface can be more specifically studied through analyzing the surface charge feature, i.e., the zeta potential. It can be seen in Fig. 10 that zeta potential of + 1.9 mV can be observed in the pure AFt sample, same to study by Plank [31]. Zeta potential is greatly reduced when NS or SF has been added. It can be deduced that the negatively charged NS and SF will squeeze the Stern layer of AFt, reducing its thickness (i.e., the zeta potential) according to the electrical double layer theory (EDL). Due to the bigger size of SF to NS, the former will result in thicker adsorption on the AFt surface, leading to a greater reduction of the zeta potential as shown in Fig. 10.

The cases in cement pore solution were simulated by saturated lime solution (pH = 12.0), and the results were also shown in Fig. 10. An increase of zeta potential can be seen in all samples due to the increase of Ca^{2+} ions. At the same time, a comparable trend can be seen after the addition of NS and SF.

4. Conclusions

This paper explored the surface adsorption characteristics of nano silica (NS) and silica fume (SF) on C$_3$A-gypsum systems, with the aim of investigating how will these adsorption features will influence the sulfate attack resistivity. The following conclusions can be drawn:

1) NS and SF can effectively improve the sulfate attack resistivity of the C$_3$A-gypsum systems due to both the compactness of the microstructure introduced by the filling effect and the reduction of the expansion potential exerted by AFt of varying size features. Comparatively, rare influence on the morphology of AFt can be resulted in SF-added samples;

2) The sulfation degree of the C$_3$A will potentially influence the sulfate attack resistivity. At a poorly sulfated system (30 wt% gypsum), AFm will be majorly formed. While AFt and AFm will jointly be formed in practically sulfated cement (86 wt% gypsum). A relatively loose microstructure can form due to the needle-like AFt rather than the

plate AFm. Moreover, AFt of short rod form in 86 wt% gypsum sample tending to swell when meeting water could also contribute to the cracking or deterioration;

3) Zeta potential results showed that NS and SF could be adsorbed onto the AFt phase. The NS can more potentially alter the morphology of AFt than SF due to its much smaller size. Moreover, the AFt morphology can rarely be modified by SF due to its bigger size that probably cannot effectively block the ion migration.

It is expected that these finding could contribute to the utilization of fine/ultra-fine SCMs utilization in cementitious materials, especially those with high amount of aluminate phases.

CRediT authorship contribution statement

Pengkun Hou: Conceptualization, Formal analysis, Investigation, Funding acquisition, Resources, Writing – original draft, Writing – review & editing. **Xinming Wang:** Methodology, Formal analysis, Data curation. **Xiangming Zhou:** Conceptualization, Funding acquisition, Supervision, Writing – review & editing. **Xin Cheng:** Conceptualization, Writing – review & editing. **Surendra P. Shah:** Conceptualization, Writing – review & editing.

Declaration of Competing Interest

The authors declare that they have no known competing financial interests or personal relationships that could have appeared to influence the work reported in this paper.

Acknowledgment

References

[1] J.J. Gaitero, I. Campillo, A. Guerrero, Reduction of the calcium leaching rate of cement paste by addition of silica nanoparticles, Cem. Concr. Res. 38 (2008) 1112–1118.

[2] Z. Li, M.-E. Fei, C. Huyan, X. Shi, Nano-engineered,, Fly Ash-Based Geopolymer Composites: An Overview, Resour. Conserv. Recycl. (2020), 105334.

[3] Y. Dhandapani, M. Santhanam, G. Kaladharan, S. Ramanathan, Towards ternary binders involving limestone additions — A review, Cem. Concr. Res. 143 (2021), 106396.

[4] V.M. John, B.L. Damineli, M. Quattrone, R.G. Pileggi, Fillers in cementitious materials — Experience, recent advances and future potential, Cem. Concr. Res. 114 (2018) 65–78.

[5] B. Lothenbach, K. Scrivener, R.D. Hooton, Supplementary cementitious materials, Cem. Concr. Res. 41 (2011) 1244–1256.

[6] P.-C. Aïtcin, Developments in the application of high-performance concretes, Constr. Build. Mater. 9 (1) (1995) 13–17.

[7] R.F. Santos, J.C.L. Ribeiro, J.M. Franco de Carvalho, W.L.E. Magalhães, L. G. Pedroti, G.H. Nalon, G.E.S.d. Lima, Nanofibrillated cellulose and its applications in cement-based composites: A review, Constr. Build. Mater. 288 (2021) 123122, https://doi.org/10.1016/j.conbuildmat.2021.123122.

[8] G. Li, Properties of high-volume fly ash concrete incorporating nano-SiO₂, Cem. Concr. Res. 34 (6) (2004) 1043–1049.

[9] L.P. Singh, S.R. Karade, S.K. Bhattacharyya, M.M. Yousuf, S. Ahalawat, Beneficial role of nanosilica in cement based materials – A review, Constr. Build. Mater. 47 (2013) 1069–1077.

[10] F. Sanchez, K. Sobolev, Nanotechnology in concrete – A review, Constr. Build. Mater. 24 (11) (2010) 2060–2071.

[11] I.F. Sáez del Bosque, M. Martín-Pastor, S. Martínez-Ramírez, M.T. Blanco-Varela, J. Biernacki, Effect of Temperature on C₃S and ₍c₎3S + Nanosilica Hydration and C-S–H Structure, J Am Ceram Soc 96 (3) (2013) 957–965.

[12] D. Kong, H. Pan, L. Wang, D.J. Corr, Y. Yang, S.P. Shah, J. Sheng, Effect and mechanism of colloidal silica sol on properties and microstructure of the hardened cement-based materials as compared to nano-silica powder with agglomerates in micron-scale, Cem. Concr. Compos. 98 (2019) 137–149.

[13] P. Hou, S. Kawashima, D. Kong, D.J. Corr, J. Qian, S.P. Shah, Modification effects of colloidal nanoSiO₂ on cement hydration and its gel property, Compos. B Eng. 45 (2013) 440–448.

[14] H. Li, H. Xiao, J. Yuan, J. Ou, Microstructure of cement mortar with nano-particles, Compos. B Eng. 35 (2004) 185–189.

[15] L.G. Baquerizo, T. Matschei, K.L. Scrivener, Impact of water activity on the stability of ettringite, Cem. Concr. Res. 79 (2016) 31–44.

[16] I. Galan, H. Beltagui, M. García-Maté, F.P. Glasser, M.S. Imbabi, Impact of drying on pore structures in ettringite-rich cements, Cem. Concr. Res. 84 (2016) 85–94.

[17] A.M. Cody, H. Lee, R.D. Cody, P.G. Spry, The effects of chemical environment on the nucleation, growth, and stability of ettringite [Ca₃Al(OH)₆]₂(SO₄)3·26H₂O, Cem. Concr. Res. 34 (2004) 869–881.

[18] A. Quennoz, K.L. Scrivener, Hydration of C₃A–gypsum systems, Cem. Concr. Res. 42 (2012) 1032–1041.

[19] J.D. Zea-Garcia, I. Santacruz, M.A.G. Aranda, A.G. De la Torre, Alite-belite-ye'elimite cements: Effect of dopants on the clinker phase composition and properties, Cem. Concr. Res. 115 (2019) 192–202.

[20] J.J. Wolf, D. Jansen, F. Goetz-Neunhoeffer, J. Neubauer, Application of thermodynamic modeling to predict the stable hydrate phase assemblages in ternary CSA-OPC-anhydrite systems and quantitative verification by QXRD, Cem. Concr. Res. 128 (2020), 105956.

[21] F. Bertola, D. Gastaldi, S. Irico, G. Paul, F. Canonico, Behavior of blends of CSA and Portland cements in high chloride environment, Constr. Build. Mater. 262 (2020), 120852.

[22] K. Scrivener, F. Martirena, S. Bishnoi, S. Maity, Calcined clay limestone cements (LC³), Cem. Concr. Res. 114 (2018) 49–56.

[23] L. Liu, W. Zhang, X. Ren, J. Ye, Z. Zhang, J. Qian, Formation, structure, and thermal stability evolution of ternesite based on a single-stage sintering process, Cem. Concr. Res. 147 (2021), 106519.

[24] K.L. Scrivener, P. Juilland, P.J.M. Monteiro, Advances in understanding hydration of Portland cement, Cem. Concr. Res. 78 (2015) 38–56.

[25] G. Geng, R.J. Myers, Y.-S. Yu, D.A. Shapiro, R. Winarski, P.E. Levitz, D. A. Kilcoyne, P.J.M. Monteiro, Synchrotron X-ray nanotomographic and spectromicroscopic study of the tricalcium aluminate hydration in the presence of gypsum, Cem. Concr. Res. 111 (2018) 130–137.

[26] X. Wang, P. Hou, P. Zhao, et al., Physicochemical effects of nanosilica on C₃A/C₃S hydration, Journal of American Ceramic Society 00 (2020) 1–14.

[27] X. Wang, P. Hou, J. Yu, X. Zhou, X. Cheng, The effects of silica fume on C₃A hydration, Constr. Build. Mater. 250 (2020) 118766, https://doi.org/10.1016/j.conbuildmat.2020.118766.

[28] S.S. Matthias Maier, A. Neißer-Deiters, N. Beuntner, Karl-Christian Thienel, Hydration of cubic tricalcium aluminate in the presence of calcined clays, J. Am. Ceram. Soc. 104 (2021) 3619–3631.

[29] M.M. Dapeng Zheng, Weipeng Feng, Waiching Tang, Hongzhi Cui, Zhijun Dong, Hydration Characteristics of Tricalcium Aluminate in the Presence of Nano-Silica, NANOMATERIALS 11 (2021) 199.

[30] A. Solanki, L.P. Singh, S.R. Karade, U. Sharma, Functionality of silica nanoparticles on hydration mechanism and microstructure of tricalcium aluminate, Constr. Build. Mater. 299 (2021), 124238.

[31] H.M. Son, S.M. Park, J.G. Jang, H.K. Lee, Effect of nano-silica on hydration and conversion of calcium aluminate cement, Constr. Build. Mater. 169 (2018) 819–825.

[32] S. Pourchet, L. Regnaud, J.P. Perez, A. Nonat, Early C₃A hydration in the presence of different kinds of calcium sulfate, Cem. Concr. Res. 39 (2009) 989–996.

[33] P. Hou, X. Wang, P. Zhao, K. Wang, S. Kawashima, Q. Li, N. Xie, X. Cheng, S. P. Shah, Physicochemical effects of nanosilica on C₃A/C₃S hydration, J. Am. Ceram. Soc. 103 (2020) 6505–6518.

[34] B. Mondal, J. Jeffery, The Crystal Structure of Triealeium Aluminate, Ca₃Al₂O₆, Acta Crtstallographica, B 31 (1975) 689–697.

[35] B. Pedersen, D. Semmingsen, Neutron Diffraction Refinement of the Structure of Gypsum, CaSO₄. 2H₂0, Acta Crtstallographica, B 38 (1982) 1074–1077.

[36] F. Goetz-Neunhoeffer, J. Neubauer, Refined ettringite (Ca₆Al₂(SO₄)₃(OH)₁₂·26H₂O) structure for quantitative X-ray diffraction analysis, Powder Diffr. 21 (2006) 4–11.

[37] S. Hajilar, B. Shafei, Structure, orientation, and dynamics of water-soluble ions adsorbed to basal surfaces of calcium monosulfoaluminate hydrates, Physical Chemtry, Chem. Phys. 20 (2018) 24681–24694.

[38] G. Renaudin, M. Francois, O. Evrard, Order and disorder in the lamellar hydrated tetracalcium monocarboaluminate compound, Cem. Concr. Res. 29 (1999) 63–69.

[39] R. Fischer, H.-J. Kuzel, Reinvestigation of the system C₄A·nH₂O, C₄A·CO₂·nH₂O, cement and Concrete Research 12 (1982) 517–526.

[40] B.Z. Dilnesa, B. Lothenbach, G. Renaudin, A. Wichser, D. Kulik, Synthesis and characterization of hydrogarnet Ca₃(AlₓFe₁₋ₓ)2(SiO₄)y(OH)₄₍₃₋y₎, Cem. Concr. Res. 59 (2014) 96–111.

[41] F. Werfel, O. Briimmer, Corundum Structure Oxides Studied by XPS, Phys. Scr. 28 (1983) 92–96.

[42] Z. Guo, Y. Wang, P. Hou, Y. Shao, X. Zuo, Q. Li, N. Xie, X. Cheng, Comparison study on the sulfate attack resistivity of cement-based materials modified with nanoSiO₂ and conventional SCMs: Mechanical strength and volume stability, Constr. Build. Mater. 211 (2019) 556–570.

[43] H.J.K.H. Pollmann, Hydration of C3A in the presence of Ca(OH)₂, CaSO₄·2H₂O and CaCO₃, Cem. Concr. Res. 21 (1991) 885–895.

[44] X. Aimin, S.L. Sarkar, Microstructural study of gypsum activated fly ash hydration in cement paste, Cem. Concr. Res. 21 (1991) 1137–1147.

[45] P.K. Mehta, Mechanism of sulfate attack on portland cement concrete—Another look, Cem. Concr. Res. 13 (1983) 401–406.

[46] J.P.M. Schönlein, Influence of PCE kind and dosage on ettringite crystallization performed under terrestrial and microgravity conditions, J. Am. Ceram. Soc. 101 (2018) 3575–3584.

[47] J. Plank, C. Schroefl, M. Gruber, M. Lesti, R. Sieber, Effectiveness of Polycarboxylate Superplasticizers in Ultra-High Strength Concrete: The Importance of PCE Compatibility with Silica Fume, J. Adv. Concr. Technol. 7 (1) (2009) 5–12.

[48] Y. Sargam, K. Wang, Influence of dispersants and dispersion on properties of nanosilica modified cement-based materials, Cem. Concr. Compos. 118 (2021), 103969.